Sādhanā (2019) 44:25
https://doi.org/10.1007/s12046-018-0988-6

Shock structures of underexpanded non-circular slot jets

T J S JOTHI[1,*] and K SRINIVASAN[2]

[1]Department of Mechanical Engineering, National Institute of Technology Calicut, Calicut 673601, India
[2]Department of Mechanical Engineering, Indian Institute of Technology Madras, Chennai 600036, India
e-mail: tjsjothi@nitc.ac.in

MS received 17 November 2017; revised 5 June 2018; accepted 20 July 2018; published online 8 January 2019

Abstract. Flow visualization studies using shadowgraph technique are carried out to investigate the shock evolution from non-circular slot jets at various under-expansion levels. The non-circular topologies considered are triangular, square and elliptic, and the circular jet is taken as the baseline case for the study. These jets are underexpanded in the pressure ratio (R) range of 2–6 corresponding to a fully expanded jet Mach number up to 1.85. Results indicate that the shock cell structures of non-circular jets strongly depend upon the initial shape of the topology. The shock structures of triangular jet have additional secondary oblique shocks that are distinct from those of other non-circular jets. Mach disk is almost absent in a shock cell structure of triangular jet, which is unlike the case of other jets used in the study. The study suggests that square jet undergoes faster diffusion process compared with the triangular jet. Axis-switching phenomenon is predicted for the elliptical jet at a distance of 3–7 equivalent diameters.

Keywords. Triangular jets; square jet; elliptic jets; shock structures; shadowgraph.

1. Introduction

Subsonic jets are correctly expanded jets at lower pressure ratios, and the static pressure along the jet is the same as the ambient pressure. However, jets issued above the critical pressure ratio undergo pressure equalizing mechanisms, thus forming the expansion fans and shocks to equilibrate the jet pressure with that of the ambient. Such jets are termed as imperfectly expanded jets that can be generated from either convergent–divergent nozzles or convergent nozzles. While the former nozzle generates both under- and over-expanded jets, the latter generates only the underexpanded jets. A schematic of an underexpanded jet is shown in figure 1. The expansion waves from the nozzle exit reflect at the jet boundary to form an oblique shock, which together constitutes a shock cell. In highly underexpanded jets, the initial oblique shocks are terminated to form a Mach disk [1]. The shock patterns of circular jets are widely investigated by several researchers in terms of their oscillations and acoustic feedback [2–4]. It is noted from the aforementioned facts that the underexpanded supersonic jets issuing from the circular nozzles are well characterized and their behaviour is well understood at different pressure ratios. However, non-circular nozzles that are asymmetric with vertices and edges in their topology are supposed to have different jet evolution. This aspect is concentrated upon in this paper and the visualization technique is used to address the flow evolution of underexpanded jets from non-circular geometries, namely the triangular, square and elliptical slot nozzles at different pressure ratios. The diffusion mechanism undergone by the different non-circular jets is discussed.

The difference in the velocity between the jet flow and ambient fluid causes the formation of a shear layer. Fluid in the shear layer rolls up due to the viscous action to form eddies. During this process, entrainment of the ambient fluid takes place throughout the shear layer. The entrainment ratio and growth rate of the shear layer depend on convective eddy velocity [5]. In the case of supersonic jets, the shear layer growth is slower compared with subsonic jets due to the compressibility effects [6]. Flow control is significant in numerous practical applications, such as in mixing enhancement, attenuating combustion instabilities and reducing noise. Non-circular nozzles are found to be an attractive passive mechanism for flow control since these jets solely depend on geometrical modifications. Among the non-circular jets, rectangular and elliptic jets are popular owing to their interesting behaviour such as enhanced mixing and entrainment, and axis switching. Other important and useful features of non-circular jets are (i) larger spread rate and thus they entrain more ambient fluid, leading to better mixing and (ii) the vertices and edges of non-circular jets help in small-scale and large-scale mixing, respectively.

Non-circular jets have an asymmetric velocity profile that modifies the shear layer evolution, and thus making the

*For correspondence

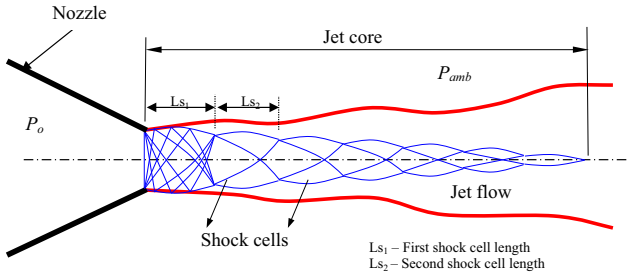

Figure 1. Schematic diagram of an underexpanded jet.

flow and shock structure complex. The presence of the vertices and edges introduces streamwise and spanwise vortices, respectively [7], and have good mixing capabilities compared with circular jets due to Biot–Savart deformation of self-induced vortices from azimuthally varying geometric profile [8]. This phenomenon leads to higher velocity from the portions of small radius of curvature compared with that along edge side. The sharp corners lead to the generation of high-frequency turbulent eddies, and the edges shed large-scale coherent structures, thus resulting in higher spread along the edge than that along vertex [9]. The small- and large-scale mixing is essential in combustion systems [10], and to improve the entrainment rate [11]. Further, the triangular jets introduce "high-instability modes into the flow via the non-symmetric mean velocity and pressure distribution around the nozzle" as discussed by Schadow *et al* [12]. When two triangular jets, namely, isosceles and equilateral shapes are compared, the former has a lower mixing rate compared with the latter [13, 14]. Investigation on axis-switching mechanism in triangular jets was performed by Koshigoe *et al* [15]. Square and rectangular jets have been under the attention of several researchers [16–19]. This jet has larger mixing rate and the reason is attributed to the four equi-spaced counter-rotating pairs of streamwise vortices from the vertices. Interestingly, Ai *et al* [20] experimentally studied the initial evolution of water jets from square geometry and discussed the penetration rates, mixing behaviour, axis switching and leapfrogging. Elliptic jets are a special case of non-circular jets since they are free from vertices and edges, and have an azimuthally varying curvature. Elliptic jets have been analysed extensively for their unique flow features such as axis switching, and enhanced entrainment [21–23]. Hussain and Husain [21] experimentally investigated the incompressible elliptic jets and concluded that the azimuthal variation in the geometry leads to non-uniform self-induction, resulting in three-dimensional jet flow structures. In addition, the azimuthal non-uniformity of the initial momentum thickness at the nozzle exit is found to vary by around 26%. This results in higher entrainment and mixing rate [24], thereby reducing the potential core to 3–4 equivalent diameters compared with a circular jet, which extends up to 5 diameters. The shear layer growth is faster along the minor axis plane compared with the major axis plane, thus causing the jet-axis to switch over along the axial distance of the jet. Quinn [25] performed mixing studies of an elliptic turbulent orifice jet (aspect ratio equal to 5) and concluded that axis switching occurs twice within 3–7 equivalent diameters, and the jet became axisymmetric at a distance of 30 equivalent diameters downstream.

Several research works exist on the flow and acoustics studies of various non-circular flows; however, most of them are related to low speeds. The flow evolution of non-circular jets is observed to be three dimensional, and characterization of such jets is necessary to understand the processes like mixing, noise generation and so on. The studies related to the non-circular jets at higher underexpanded pressure ratios are found to be limited. Therefore, in an attempt to understand the flow physics of non-circular jets at higher pressure ratios, the shadowgraph flow visualization technique is used in the current study. The literature related to the visualization of non-circular slot jets are noted to be scarce, and thus the present work demonstrates the evolution of shock cells from equilateral triangular, square and elliptic orifices. Moreover, the visualization is carried along two planes of the jet flow to understand the effect of orientation on shock cell structures.

2. Experimental set-up and procedure

2.1 *Experimental set-up*

Compressed air is used as the jet fluid for visualization studies, and is generated using a 150 HP motor, and is stored in a tank of 20 m^3 capacity. Using a 4-in. pipeline, the compressed air is brought to the settling/plenum chamber. The orifice holder with required orifices is attached to the end of the settling chamber. A schematic of the test facility is shown in figure 2. The settling chamber is large enough to hold the air at stagnation and is provided with coarse and fine meshes to reduce the turbulence in the flow. The pressure ratio R (ratio of stagnation pressure to ambient pressure) of the jet flow is varied in the range $2 \leq R \leq 6$. The various non-circular geometries fabricated are equilateral triangular, square and elliptic along with the circular geometry, and the corresponding dimensions are shown in terms of the radius of a circular orifice in figure 3(a). The required shapes are engraved in a mild steel plate of 73 mm diameter and 2 mm thickness at the centre using a wire cut *electrical discharge machining* process. It is to be noted that the orifices eliminate the azimuthally varying boundary layer [21], which are prominent in conventional nozzles as described by Quinn and Marsters [26]. All orifices have the same exit area of ≈ 78.5 mm^2, and thus the equivalent diameter (D_e) of non-circular orifices is the same as that of a circular orifice, which is 10 mm. This parameter is introduced by Hussain and Husain [21] and is widely used for elliptic jets. The orifice disks are mounted

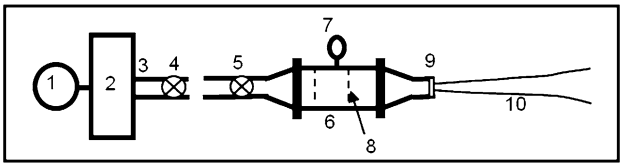

1 - Air compressor
2 - Storage tank
3 - Pipe line
4 - Gate valve
5 - Pressure regulating valve
6 - Settling chamber
7 - Pressure gauge
8 - Wire mesh screen
9 - Orifice holder
10 - Jet flow

Figure 2. Schematic of the experimental test facility.

in a disk-holder as shown in figure 3(b), which is in turn connected to the settling chamber. The periphery of the orifice plate is beaded with a thin rubber lining to ensure proper grip and to prevent air leakage.

The shadowgraph arrangement used to capture the shock cell features of circular and non-circular slot jets is shown in figure 4(a). Light from a projector is used as a point source to illuminate the jet flow-field. This light passes through a biconvex lens located at twice its focal length from the point source. The lens is positioned at a distance of around 5 cm from the jet flow. Albeit the light beam is non-collimated, as the distance between the jet flow and the lens is small, the images are expected to give the correct representation of the density gradient. The shadowgraph images are captured sequentially using a high-speed digital camera (Mikrotron Model No. 1302 CMOS Type). Due to the asymmetry in the non-circular jets, visualization is carried along different planes. Triangular and square jets are visualized along the edge and vertex planes and elliptic jets are visualized along the major and minor axes planes as indicated in figure 4(b). The normalized shock cells lengths are expected to be in the uncertainty range of ± 0.02.

3. Results and discussion

The shock cell structures of circular and non-circular jets are visualized and images are procured. Initially, the shock cell images captured from the circular orifice and nozzle are compared, followed by a discussion over the shadowgraph images of non-circular jets viewed along various planes. All the images showing the shock cell structures represent the jet flow from left to right.

3.1 *Shock structures of circular jets*

Figure 5 compares the shock cell structures of a circular jet issuing out from the orifice and nozzle at different pressure ratios. It is observed from the shadowgraph images that shock cells from orifice jets appear to be hazy while the shadowgraph images of nozzle jets are clear and sharp albeit both images are obtained for similar conditions and

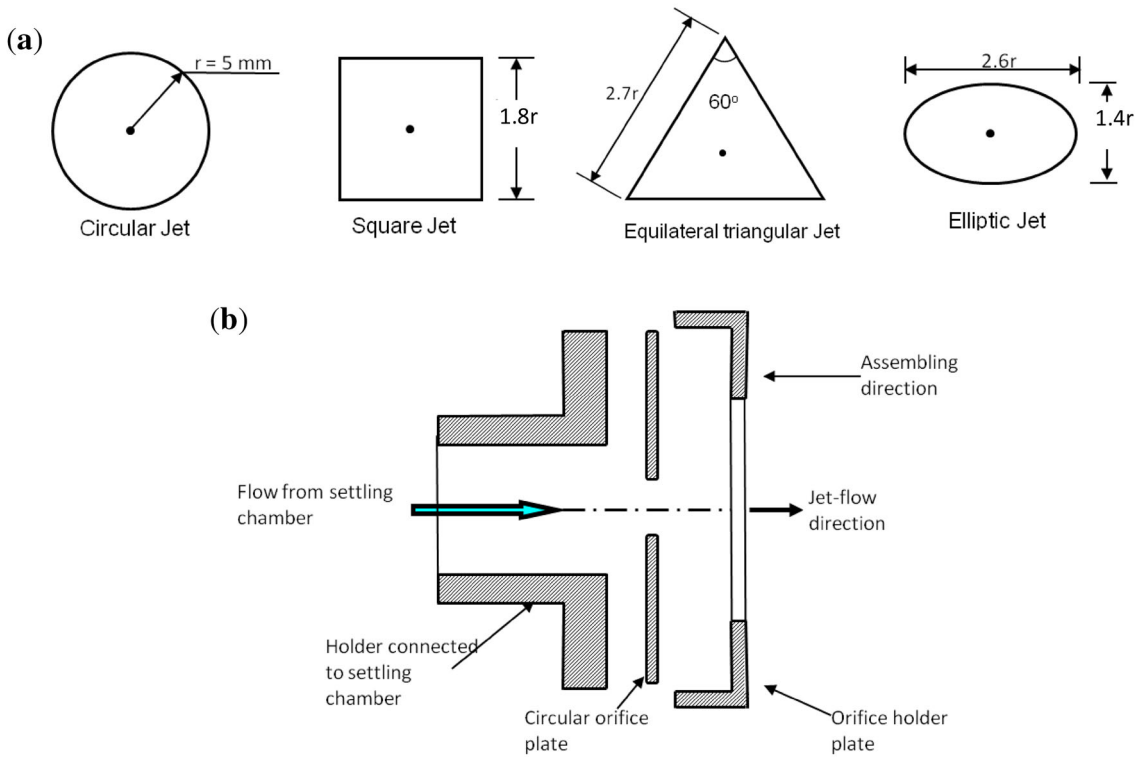

Figure 3. (**a**) Circular and non-circular orifices. (**b**) Orifice holder.

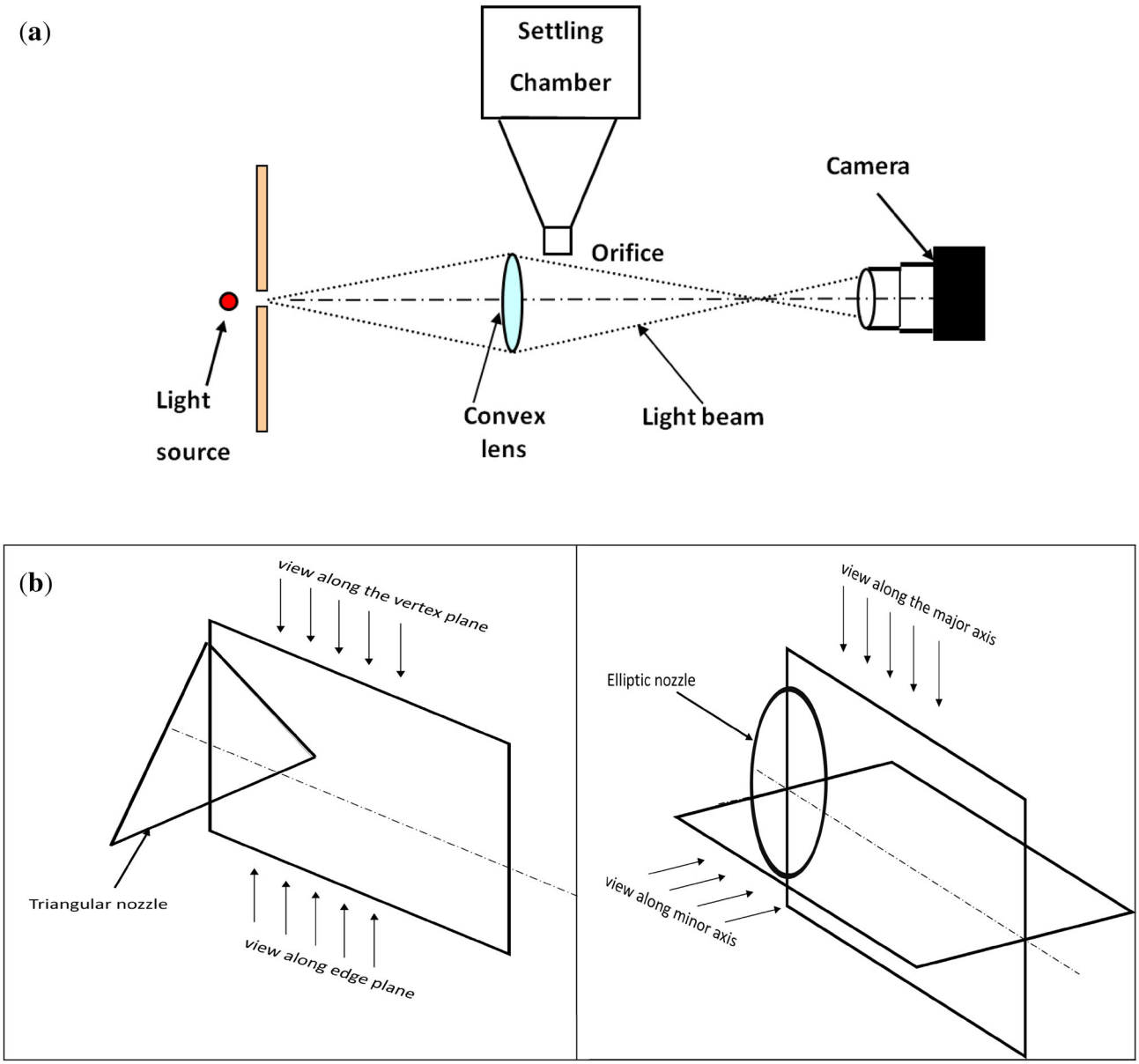

Figure 4. (**a**) Schematic of shadowgraph arrangement and (**b**) description of image acquisition for topologies having edge and vertex, and elliptic jet along major- and minor-axis.

with the same test facility. The haziness in the orifice jet images may be probably due to the higher turbulence level in the orifice jets than that issued from the nozzle [27]. Figure 6 shows the shadowgraph images of circular orifice jet at pressure ratios of 2–6. The images reveal that the Mach disk appears at $R = 3$ and is intense at $R = 6$. The number of shock cells is the highest at $R = 2$ having smaller shock cell lengths, while the cell length is seen to increase at higher pressure ratios. Further, the second shock cell at $R = 6$ seems to diffuse due to higher turbulence levels. The fringe pattern at the centre of the images is due to the refraction in the lens superimposed with the shock cell images. Figure 7 shows the normalized shock cell length variation with pressure ratio for first and second shock cells (see figure 1 for the illustration of shock cell length) of circular slot jets. The shock cell lengths are seen to increase with pressure ratio. The obtained shock lengths are compared to the model proposed by Norum and Seiner [28] for the average shock cell spacing as $L_s = 1.1\beta D_e$, where $\beta = \sqrt{(M_j^2 - 1)}$ and D_e is the nozzle exit diameter. The shock cell lengths are found to be in congruence with the proposed model as observed in figure 7. At all the pressure ratios, the lengths of the second shock cell are higher compared with that of the first shock cells.

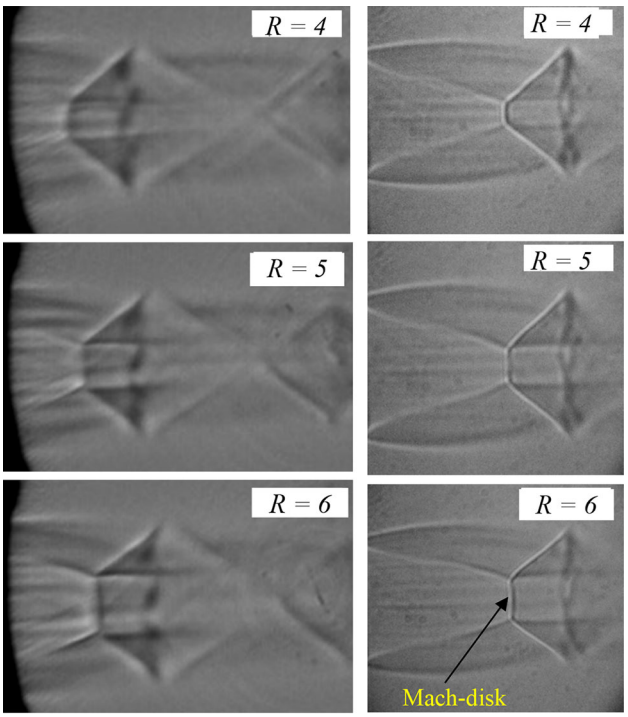

Figure 5. Comparison of shadowgraph images of circular jets issuing from (**a**) orifice slot and (**b**) convergent nozzle at different nozzle pressure ratios.

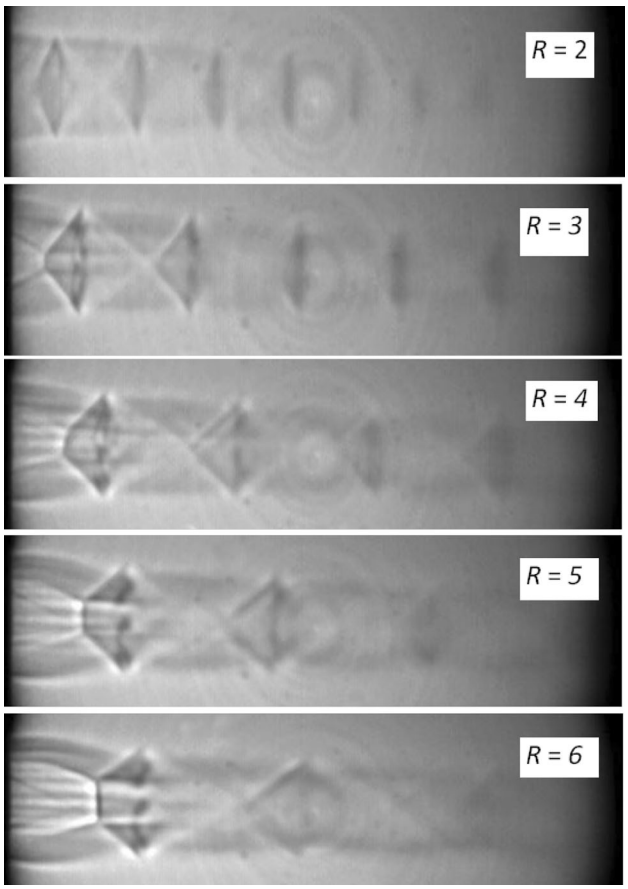

Figure 6. Shadowgraph images of circular slot jet at different pressure ratios.

3.2 *Shock structures of non-circular jets*

3.2a *Triangular and square jets*: Figure 8 shows the shadowgraph images of the equilateral triangular slot jet along the edge and vertex planes for pressure ratio ranging from 2 to 6. Preliminary observation reveals that the shock structures from triangular jets have multiple oblique shocks that are unlikely in the case of circular jets. Figures also indicate that the shock features along both the planes of triangular jets are not identical. This is due to the asymmetric density distribution across the cross-section of the jet flow. Thus the flow issuing from the vertex of the triangular jet is expected to have a higher density than that issued from the edge [8]. The view along the vertex plane shows the presence of streamwise vortices in the flow-field (figure 8b). The cartoon representing the flow structures from vertex and edge of a triangular orifice is shown in figure 9 for better illustration. Weak oblique shocks are seen in the triangular jet due to the reflections at the jet boundary (figure 8a) at higher pressure ratios. This may be understood as the propagation of coherent structures at supersonic velocities, thus generating the Mach waves. At higher pressure ratios, the shock cells of triangular jet become complex, which may be due to the azimuthal variation in the shock cell structure. For instance, at pressure ratios of 5 and 6, the second shock cell seems to be initiated before the termination of the first shock cell (figure 8a). Moreover, for $R > 4$, there exists a secondary shock in addition to the regular shock cell and gets intense with an increase in pressure ratio. Since this is immediately adjoining the primary shock cell region, it is conjectured that this is due to the supersonic speed of instability waves in the shear layer. Unlike the case of circular jets, Mach disk is either weak or absent for triangular jets at higher pressure ratios (figure 8a). This suggests that triangular nozzle topology is effective in restructuring the shock cells compared with the circular nozzles. Further, the absence of Mach disk lowers the diffusion of the supersonic jet, and in conclusion, triangular geometries may not be effective in diffusing the supersonic jets at a larger rate. This can be observed from figure 8, where the second to fourth shock cells are eminent at highest pressure ratios.

Figure 10 show shadowgraph images of the square slot jet along the edge and vertex planes for various pressure ratios. Along the edge plane (figure 10a), the flow diverges from the jet-centreline at all pressure ratios. This observation is in contrast with the images along the vertex plane, where the flow is seen converging towards the jet-centreline (figure 10b). These effects may be due to the topology of the square nozzle that comprises four edges and vertices, which is expected to have different flow characteristics.

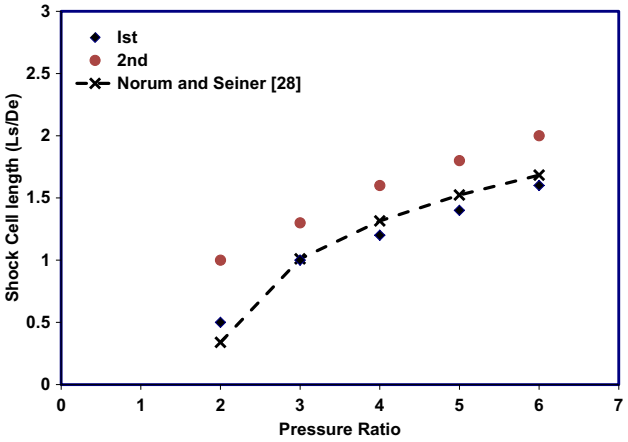

Figure 7. Shock cell length variation with pressure ratios for circular slot jet.

Along the vertex plane, the flow emerging from corner tends to induce into the main flow, thus making the jet flow converge, while along the edge, the shear layer may grow along the jet direction, and thus the jet seems to diverge [16]. The width of the shock structures is observed to be higher along the edge plane compared with the vertex plane; however, their lengths are almost identical. At higher pressure ratio of $R > 5$, a Mach disk is observed in the shock structure of square jet, which is absent for the equilateral triangular jet. This results to an important conclusion that albeit the triangular and square topologies belong to the family containing the vertices and edges, the diffusion is stronger in the latter jet compared with the former due to the presence of Mach disk. This fact can also be observed in figure 10, where the second and further shock cells in square jets are weaker compared with the triangular jets at the same pressure ratio. Further, weak streamwise vortices are presumed along the vertex plane of the square jet (figure 10b), while the same is stronger in case of triangular jets (figure 8b). The reason for this is attributed to the internal angle of the topology, where the smaller internal angle leads to the stronger streamwise

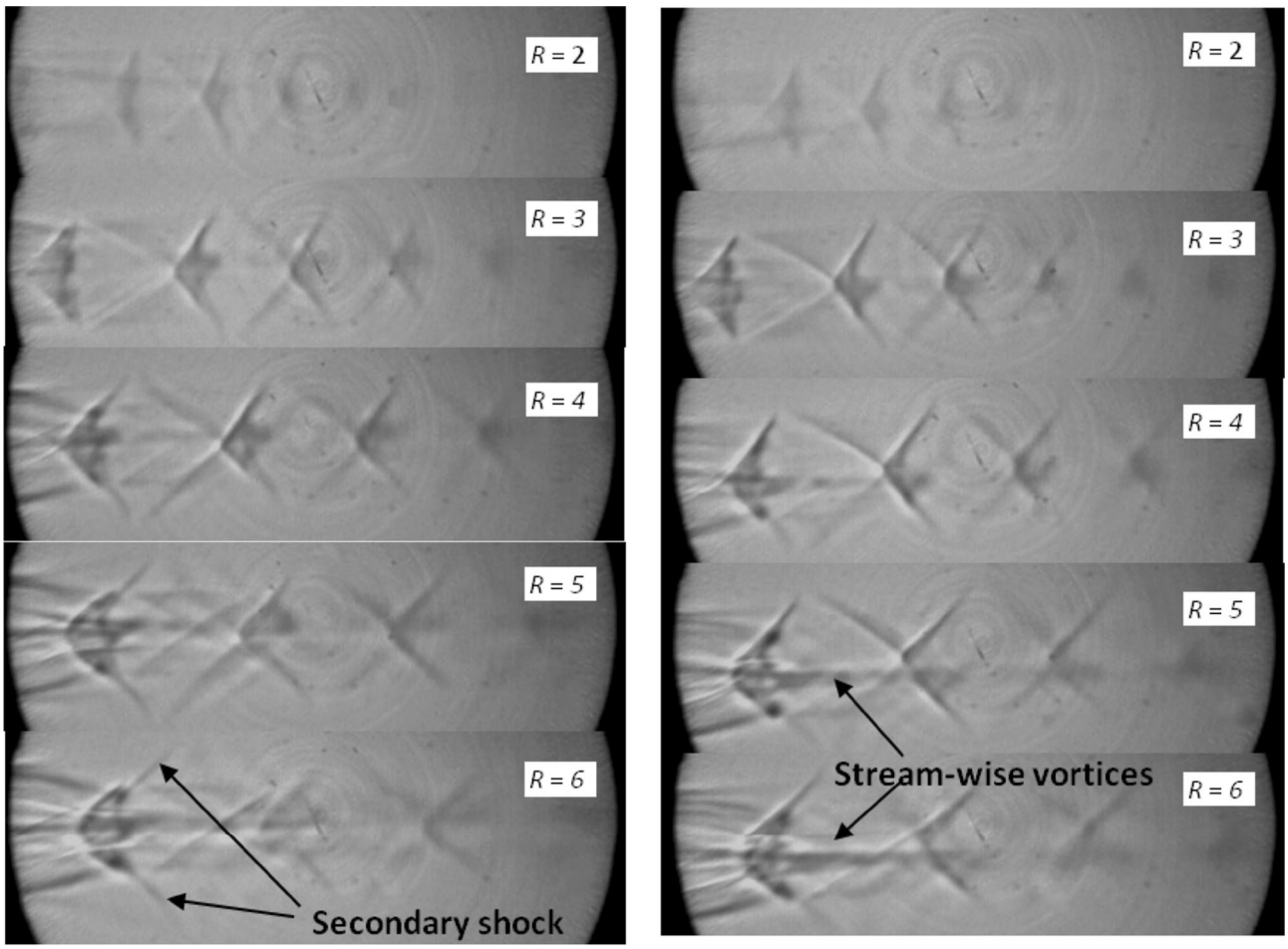

(**a**) (**b**)

Figure 8. Shadowgraph images of equilateral triangular jet at various pressure ratios, viewed along the (**a**) edge plane and (**b**) vertex plane.

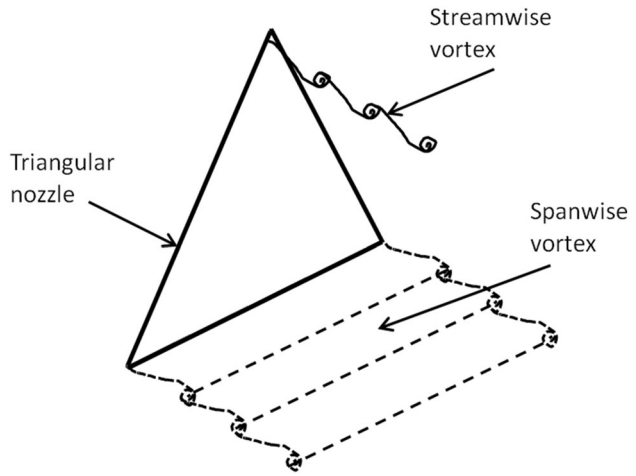

Figure 9. Cartoon representing the streamwise and spanwise vortices from the triangular jet.

vortices compared with that of the larger ones. Hence, the equilateral triangular geometry with an internal angle of 60° generates stronger streamwise vortices in the flow-field compared with the square geometry having the internal angle of 90°. In addition, as the number of vertices in the geometry increases, the jet dissipates faster, and the square jet seems to attain faster symmetry than the triangular jets [29].

3.2b *Elliptic jet*: This section describes the shadowgraph images of elliptic jet along the major- and minor-axis planes shown in figure 11. The first shock cell of elliptic jets looks similar to that of a circular jet; however, the consecutive shock cells have higher width unlike the case of a circular jet. The shock cell length and width of the elliptic jet, when viewed along the minor axis plane (figure 11a), are higher compared with that along the major axis plane (figure 11b). The reason could be the different entrainment rates along the periphery of an elliptic nozzle [24]. Further, a smaller radius of curvature of elliptic jet introduces vortices, which get self-induced in the jet stream [8] and propagate at higher velocities, thereby increasing the shock cell length and width (figure 11a). The second shock cell viewed along the major axis plane (figure 11b) is observed to have higher clarity compared with that viewed along the minor axis plane (figure 11a) for pressure ratios

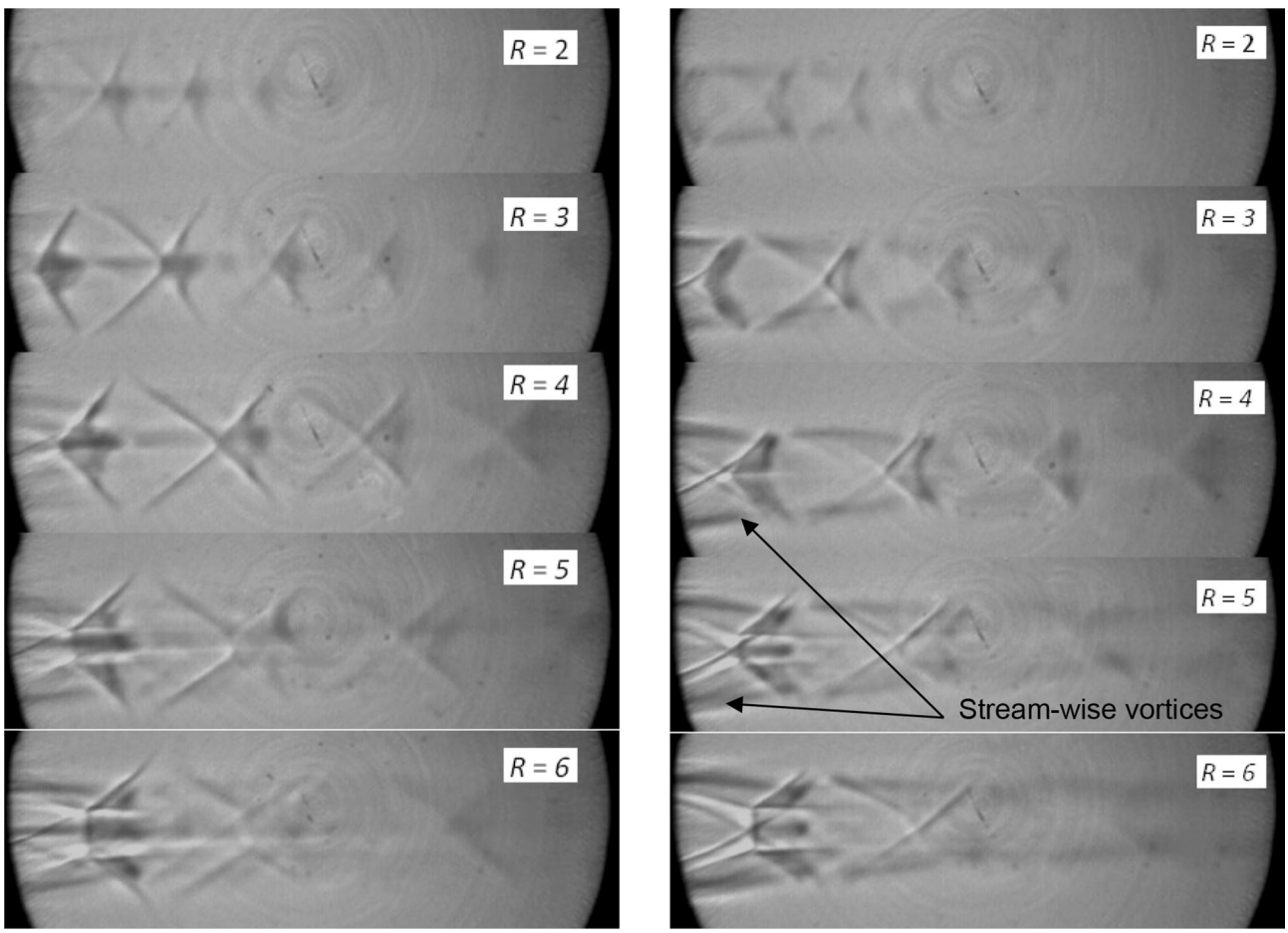

(**a**) (**b**)

Figure 10. Shadowgraph images of square jet at various pressure ratios, viewed along the (**a**) edge plane and (**b**) vertex plane.

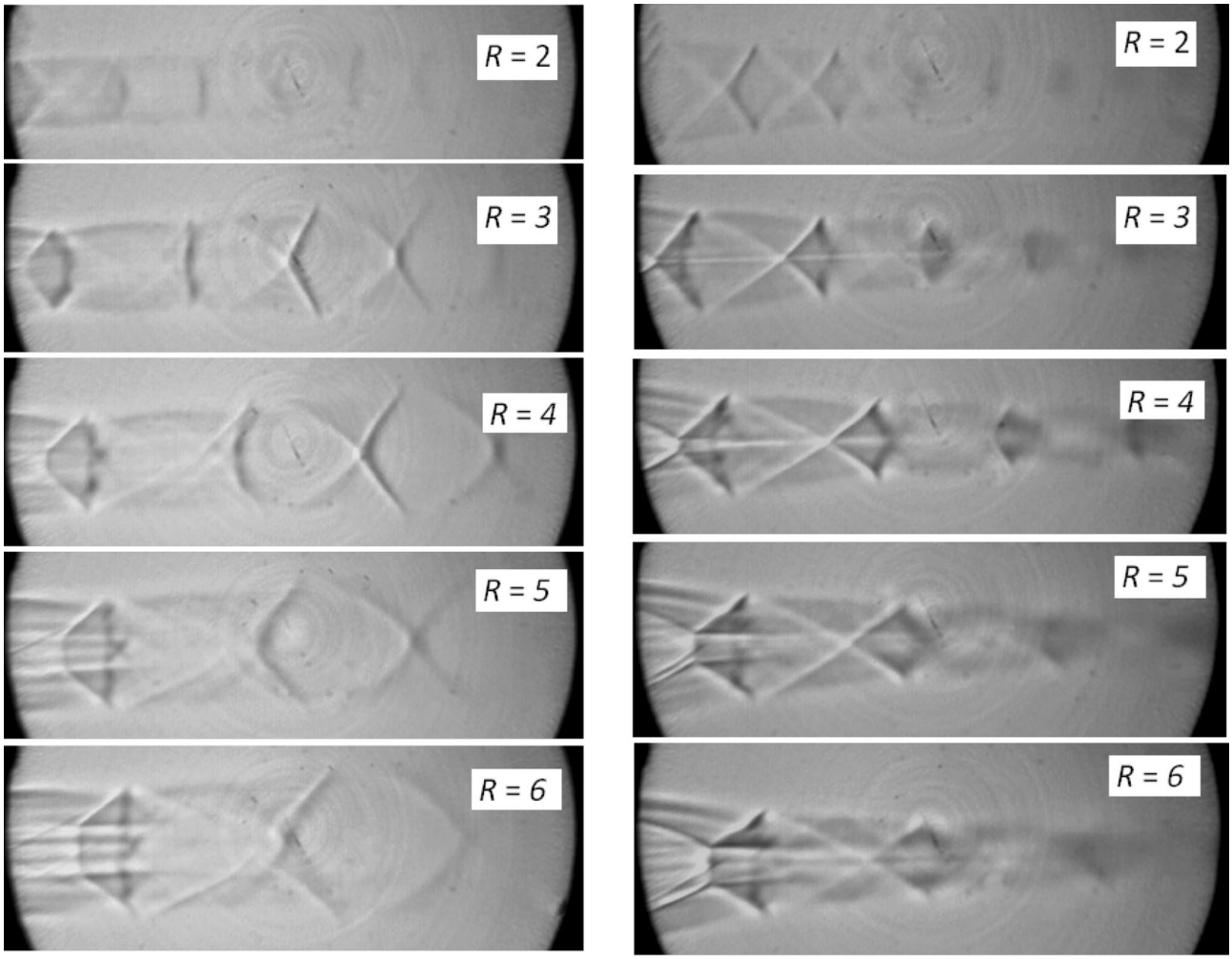

Figure 11. Shadowgraph images of elliptic jet at various pressure ratios, viewed along the (**a**) minor axis plane and (**b**) major axis plane.

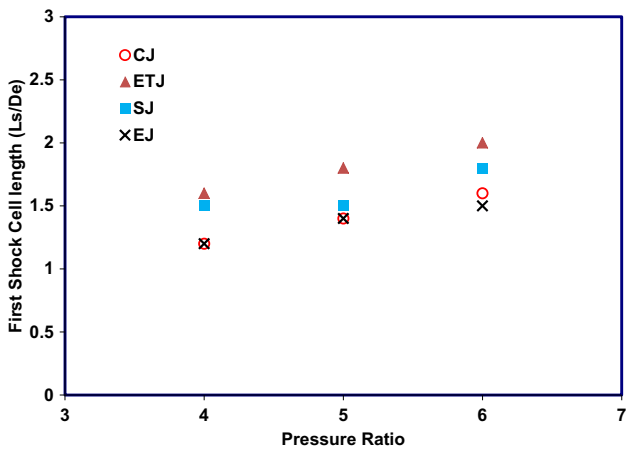

Figure 12. Normalized first shock cell length variation with pressure ratios for various jets.

of 3–5. Consecutively, the third shock cell is seen to have clarity when viewed along the minor axis plane. This switch in the clarity from the second to third shock cell in two different planes may be attributed to the axis-switching phenomenon in elliptic jets at an axial distance of around 3–7 equivalent diameters [21–23].

Figure 12 compares the first shock cell lengths normalized with the orifice diameter for circular and non-circular jets. Interestingly, the shock cell lengths of the circular and elliptic jets are almost similar since they do not have any sharp corners in their geometry. Among the non-circular jets, the triangular jet has the largest shock cell length, which could be attributed to the lower diffusion mechanism as discussed in the previous section. The shock cell length of the square jet is between those of the triangular and circular jets, therefore, agreeing with the facts that square jet combines the advantages of both circular and non-circular jets.

4. Conclusion

An investigation has been carried out to analyse the shock cells of non-circular slot jets, namely the square, equilateral triangular and elliptic jets, and compared to those of a circular jet at different under-expansion levels. Shadowgraph technique is employed to capture the shock structures of the jets. Results indicate that the Mach disk in the triangular jet is either weak or almost absent at higher pressure ratios. Further, the triangular topology is observed to restructure the shock cell evolution by addition of secondary shocks. The square jet has a Mach disk similar to that of a circular jet, and the presence of four vertices leads to the diffusion of the supersonic jet at a larger rate compared with the triangular jet. In case of elliptic jets, the width of the shock cell is considerably larger along the major axis compared with that along the minor axis. The images indicate an axis-switching mechanism in the elliptic jet flow-field within 3–7 diameters. Therefore, this study concludes that the square jet combines the advantages of both the circular and non-circular jets, by forming the Mach disk and utilizing the effects of vertices and edges, respectively, for faster diffusion of supersonic jets.

References

[1] Christ S, Sherman P M and Glass D R 1966 Study of the highly underexpanded sonic jet. *AIAA J.* 4: 68–71
[2] Powell A 1953 On the mechanism of choked jet noise. *Proc. Phys. Soc. B* 66: 1039–1056
[3] Adamson Jr T C and Nicholls J A 1959 On the structure of jets from highly underexpanded nozzles into still air. *J. Aerosp. Sci.* 26:16–24
[4] Hammit A G 1961 The oscillation and noise of an overpressure sonic jet. *J. Aerosp. Sci.* 28: 673–680
[5] Dimotakis P E 1986 Two-dimensional shear-layer entrainment. *AIAA J.* 24: 1791–1796
[6] Papamoschou D and Roshko A 1988 The compressible turbulent shear layer: an experimental study. *J. Fluid Mech.* 197: 453–477
[7] Srinivasan K and Rathakrishnan E 2000 Studies on polygonal slot jets. *AIAA J.* 38: 1985–1987
[8] Gutmark E J and Grinstein F F 1999 Flow control with non-circular jets. *Annu. Rev. Fluid Mech.* 31: 239–272
[9] Quinn W R 1990 Mean flow and turbulence measurements in a triangular turbulent free jet. *Int. J. Heat Fluid Fl.* 11: 220–224
[10] Gutmark E, Schadow K C and Wilson K J 1991 Subsonic and supersonic combustion using non-circular injectors. *J. Propul. Power* 7: 240–249
[11] Vandsburger U and Ding C 1995 The spatial modulation of a forced triangular jet. *Exp. Fluids* 18: 239–248
[12] Schadow K C, Gutmark E, Parr D M and Wilson K J 1988 Selective control of flow coherence in triangular jets. *Exp. Fluids* 6: 129–135
[13] Quinn W R 2005 Measurements in the near flow field of an isosceles triangular turbulent free jet. *Exp. Fluids* 39: 111–126
[14] Quinn W R 2005 Near-field measurements in an equilateral triangular turbulent free jet. *AIAA J.* 43: 2574–2585
[15] Koshigoe S, Gutmark E, Schadow K C and Tubis A 1989 Initial development of non-circular jets leading to axis switching. *AIAA J.* 27: 411–419
[16] Quinn W R 1992 Turbulent free jet flows issuing from sharp-edged rectangular slots: The influence of slot aspect ratio. *Exp. Therm. Fluid Sci.* 5: 203–215
[17] Quinn WR 1992 Streamwise evolution of a square jet cross-section. *AIAA J.* 30: 2852–2857
[18] Quinn W R and Militzer J 1988 Experimental and numerical study of a turbulent free square jet. *Phys. Fluids* 31: 1017–1025
[19] Grinstein F F, Gutmark E and Parr T 1995 Near field dynamics of subsonic free square jets: a computational and experimental study. *Phys. Fluids* 7: 1483–1497
[20] Ai J J, Yu S C M, Law A W K and Chua L P 2005 Vortex dynamics in starting square water jets. *Phys. Fluids* 17: 1–12
[21] Hussain F and Husain H S 1989 Elliptic jets. Part 1. Characteristics of unexcited and excited jets. *J. Fluid Mech.* 208: 257–320
[22] Husain H S and Hussain F 1991 Elliptic jets. Part 2. Dynamics of coherent structures: pairing. *J. Fluid Mech.* 233: 439–482
[23] Husain H S and Hussain F 1993 Elliptic jets. Part 3. Dynamics of preferred mode coherent structure. *J. Fluid Mech.* 248: 315–361
[24] Ho C M and Gutmark E 1987 Vortex induction and mass entrainment in a small aspect ratio elliptic jet. *J. Fluid Mech.* 179: 383–405
[25] Quinn W R 1989 On mixing in an elliptic turbulent free jet. *Phys. Fluids A* 1: 1716–1722
[26] Quinn W R and Marsters G F 1985 Upstream influence on turbulent jet from cruciform nozzles. *Aeronaut. J.* 89: 55–58
[27] Mi J, Nathan G J and Nobes D S 2001 Mixing characteristics of axisymmetric free jets from a contoured nozzle, an orifice plate and a pipe. *J. Fluids Eng.* 123: 878–883
[28] Norum T D and Seiner J M 1982 Broadband shock noise from supersonic jets. *AIAA J.* 20: 68–73
[29] Jothi T J S and Srinivasan K 2008 Acoustic characteristics of non-circular slot jets. *Acta Acust. United Acust.* 94: 229–242